Published in final edited form as:
J Magn Reson Imaging. 2007 March ; 25(3): 540–547. doi:10.1002/jmri.20816.

R2* Imaging of Transfusional Iron Burden at 3T and Comparison with 1.5T

Pippa Storey, PhD[1,2,*], **Alexis A. Thompson, MD**[2,3], **Christine L. Carqueville, BA**[4], **John C. Wood, MD, PhD**[5,6], **R. Andrew de Freitas, MD**[2,7], and **Cynthia K. Rigsby, MD**[2,4]

[1]Radiology Department, Evanston Northwestern Healthcare, Evanston, Illinois, USA.

[2]Feinberg School of Medicine, Northwestern University, Chicago, Illinois, USA.

[3]Department of Pediatrics, Children's Memorial Hospital, Chicago, Illinois, USA.

[4]Department of Medical Imaging, Children's Memorial Hospital, Chicago, Illinois, USA.

[5]Departments of Radiology and Pediatrics, Division of Cardiology, Children's Hospital of Los Angeles, Los Angeles California, USA.

[6]Keck School of Medicine, University of Southern California, Los Angeles, California, USA.

[7]Department of Cardiology, Children's Memorial Hospital, Chicago, Illinois, USA.

Abstract

Purpose: To determine normative R2* values in the liver and heart at 3T, and establish the relationship between R2* at 3T and 1.5T over a range of tissue iron concentrations.

Materials and Methods: A total of 20 healthy control subjects and 14 transfusion-dependent patients were scanned at 1.5T and 3T. At each field strength R2* imaging was performed in the liver and heart.

Results: Normative R2* values in the liver were estimated from the control group to be 39.2 ± 9.0 second^{-1} at 1.5T and 69.1 ± 21.9 second^{-1} at 3T. Normative cardiac values were estimated as 23.4 ± 2.2 second^{-1} at 1.5T and 30.0 ± 3.7 second^{-1} at 3T. The combined R2* data from patients and control subjects exhibited a linear relationship between 3T and 1.5T. In the liver, the line of best fit to the 3T vs. 1.5T data had a slope of 2.00 ± 0.06 and an intercept of −11 ± 4 second^{-1}. In the heart, it had a slope of 1.88 ± 0.14 and an intercept of −15 ± 4 second^{-1}.

Conclusion: These preliminary data suggest that the iron-dependent component of R2* scales linearly with field strength over a wide range of tissue iron concentrations. The incidence of susceptibility artifacts may, however, also increase with field strength.

Keywords

MRI; R2*; T2*; iron overload; thalassemia; 3T

PATIENTS WITH CERTAIN HEREDITARY anemias such as thalassemia major require regular blood transfusions to maintain adequate hemoglobin levels. However, the body has limited capacity to excrete iron, so frequent transfusions result in iron accumulation, particularly in the liver, spleen, endocrine organs, and heart. Iron is sequestered within

[*]Address reprint requests to: P.S., Radiology Department, Walgreen Building, G507, Evanston Hospital, 2650 Ridge Avenue, Evanston, IL 60201. p-storey@northwestern.edu.

intracellular lysosomes in the form of ferritin, which subsequently degrades into hemosiderin. When this storage mechanism becomes saturated or compromised, free iron levels increase within the cells, causing oxidative damage through the production of hydroxyl radicals (1,2). Tissue damage in the myocardium causes conduction disturbances and left ventricular hypertrophy. The resulting cardiac complications, including ventricular arrhythmias and congestive heart failure, remain the leading cause of death in patients with thalassemia major (3).

To minimize myocardial injury, transfusion-dependent patients must undergo lifelong chelation therapy and periodic monitoring of iron burden (4). Since much of the body's excess iron is deposited in the liver, hepatic iron concentration has traditionally been used as a surrogate for total body iron and measured using liver biopsy. However, biopsy is invasive and therefore inappropriate for regular monitoring. Also, its accuracy may be limited by uneven iron distribution and hepatic fibrosis, which is common in thalassemia as a result of iron-mediated tissue damage and hepatitis C viral infection (5). Furthermore, evidence suggests that liver iron concentration is an incomplete predictor of myocardial iron load (6,7).

MRI offers a noninvasive alternative for assessment of tissue iron levels, and can be used to monitor iron burden in the heart as well as the liver. Since hemosiderin is paramagnetic, it produces local perturbations in the magnetic field, which increase proton relaxation rates. Although hemosiderin affects both longitudinal and transverse relaxation rates, its transverse relaxivity is much higher than its longitudinal relaxivity, due to the large size of the hemosiderin molecules and their clustered distribution within intracellular lysosomes (8,9).

Most MRI approaches to iron quantification, therefore, involve measuring the transverse relaxation rates, R2 (= 1/T2) or R2* (= 1/T2*). R2* mapping is typically easier to implement and quicker to perform, especially in the heart, since gradient-echo images can be acquired within a single breathhold. However, it is sensitive to large-scale magnetic field inhomogeneities, which can arise from poor shimming and magnetic susceptibility differences between organs. R2 mapping uses spin-echo techniques, and is thus insensitive to macroscopic field inhomogeneities but is inherently much slower to perform. It has been implemented in the liver using a free-breathing approach (10) and at extremely low resolution with breathholding (11). It can be applied to the heart, however, only with the aid of both respiratory and cardiac triggering (12,13). It is also more sensitive to through-plane motion, which can cause anomalous signal decay through incomplete re-focusing.

Both R2 and R2* have been shown to provide accurate estimates of hepatic iron over the entire clinically relevant range (11). Evidence suggests that R2 remains highly specific for iron concentration even in the presence of hepatic fibrosis (14). While the relationships between hepatic iron concentration and MRI relaxation rates are now well established at 1.5T (10,11), they have not yet been investigated at 3T. With the increasing availability of 3T scanners, there is a growing need to assess the practicality of evaluating iron burden at 3T. Since relaxation rates are in general field-dependent, their relationship to tissue iron concentration must be reevaluated at 3T, either directly by means of biopsy, or indirectly through calibration against 1.5T values. The goal of this study was to determine normative R2* values in the liver and heart at 3T, and to establish the relationship between R2* values at 3T and 1.5T over a range of tissue iron concentrations.

MATERIALS AND METHODS

Subject Cohort

A total of 20 healthy control subjects and 14 transfusion-dependent patients were enrolled in the study, which had received prior approval from the Institutional Review Boards of both

participating hospitals. All adult subjects provided written informed consent before taking part; minors gave assent and their parents provided written informed consent. The control group included 10 men and 10 women, aged 26.1 ± 6.6 years (range 20–41 years). The patient cohort comprised six men and eight women, aged 24.1 ± 9.4 years (range 12–44 years), of whom 11 had β-thalassemia, one had hemoglobin E (HBe)/β-thalassemia, one had Δ-β thalassemia, and one had congenital dyserythropoietic anemia. Three of the patients completed the imaging protocol twice, at intervals of 175, 195, and 345 days.

Imaging Protocol

Each subject was scanned at 1.5T and 3T with an intervening break of less than 15 minutes. The scans were conducted on GE Healthcare Signa Twinspeed systems, using a cardiac phased-array coil at 1.5T and a torso phased-array coil at 3T. The software platform on each scanner was upgraded from EXCITE II (version 11.0) to HD (version 12.0) midway through the study. The 3T system was further upgraded to HDx (version 14.0) toward the end of the study.

R2* imaging was performed in the liver and heart at both field strengths. A breathheld multiple gradient echo (MGRE) technique was used to acquire a series of images with increasing echo times (TE) at each slice position. The MGRE sequence was run with a flip angle of 20° and a readout bandwidth of 83.3 kHz. In the liver, 16 echoes were acquired in a single axial slice, using six averages (NEX) and a matrix size of 128 × 128, giving an echo spacing of $\Delta TE \approx 1.0$ msec. The echo time of the first echo was between 1.2 and 2.0 msec, depending on the software version, and the repetition time was $TR \approx 20$ msec.

In the heart, a gated segmented version of the MGRE sequence was applied. It was run in four midventricular short axis slices, using eight echoes, NEX = 1, and a matrix size of 192 × 160, giving an echo spacing of $\Delta TE \approx 1.4$ msec. The echo time of the first echo was between 1.6 and 2.0 msec, depending on the software version, and the repetition time was $TR \approx 13$ msec. Pulse gating was used to synchronize the data acquisition to end systole, when the myocardium is thickest and its motion is minimal. The number of views per segment (i.e., the number of *k*-space lines per cardiac cycle) was chosen as a function of the heart rate and breathholding capability of the subject.

On the HD and HDx platforms, a small-volume shim technique was used to optimize the gradient settings locally over the liver or heart as appropriate. This feature was not available on the EXCITE II platform. Because the upgrade from EXCITE II to HD did not occur until about midway through the study, the majority of the control subjects (19 out of 20) were scanned without the small volume shim at one or both field strengths. A total of six of the 17 patient studies (including the repeat visits) were also performed without the small volume shim.

After each acquisition the images were examined on the console, either by visual inspection or using the built-in FuncTool software. If the signal in the tissue of interest (liver or myocardium) appeared to have dropped to near the noise level by the second or third echo, the acquisition was repeated using a single-echo technique in order to sample the decay curve more finely over the short TE range. In the single-echo approach, several images were acquired during separate breathholds using a conventional fast gradient echo sequence. The echo time was set to its minimum value for the first image, and then incremented manually by a fraction of a millisecond ($\Delta TE = 0.1$ or 0.2 msec) between each of the following acquisitions. The echo time was increased until the tissue of interest appeared dark. Care was taken throughout to maintain constant values for the repetition time and the prescan parameters (receiver gain, transmitter gain, shim settings, and center frequency). A bandwidth of 83.3 kHz was chosen to achieve the shortest possible TE. In the liver, the sequence was run in a single axial slice with a flip angle of 10°, TR = 10 msec, NEX = 8, and matrix size = 128 × 128, giving a minimum echo time of $TE_{min} \approx 0.8$ msec. When a single-echo approach was needed in the heart, a gated

segmented fast gradient echo sequence was used. It was applied in a single midventricular short axis slice with a flip angle of 10°, TR = 4.4 msec, NEX = 1, and matrix size = 192 × 160, giving a minimum echo time of $TE_{min} \approx 1$ msec.

Image Analysis

R2* values were calculated offline using customized routines written in MATLAB (Natick, MA). About 10 regions of interest (ROIs) were chosen in the liver, avoiding all visible vessels. In the heart, up to three ROIs were chosen per slice. They were placed in the interventricular septum to minimize the effect of susceptibility differences between the heart and lung. Where data had been acquired with the MGRE sequence, the ROIs were propagated automatically through all the images in the series. Where the single-echo technique had been used, the positions of the ROIs could be adjusted to account for differences in breathholding position from image to image.

For each ROI a single value of R2* was calculated as follows. The mean intensity within the ROI was evaluated for each image in the series and plotted as a function of TE. In cases of rapid signal decay, the data were truncated at the point where the mean intensity fell below about twice the noise level (15). R2* was then calculated by fitting the intensity data to a monoexponential decay using a nonlinear Levenberg-Marquardt algorithm.

In addition to the ROI analysis, maps of R2* were generated by applying the same fitting procedure, pixel by pixel. To avoid misregistration problems between images, maps were produced only for data acquired in a single breathhold using the MGRE technique.

Statistical Analysis

The mean and SD of R2* over all the ROIs were evaluated in the liver and heart for each subject and at each field strength. The mean was used as a best estimate of R2* in each case, and the SD was used as a measure of uncertainty. The 3T values for all participants (patients and control subjects) were plotted against the corresponding 1.5T values, and the data were fitted to a straight line, taking into account the uncertainties in both the 3T and 1.5T values. To avoid the possibility that erroneous data arising from susceptibility artifacts might disproportionately affect the results, certain points were classified as outliers and excluded from the analysis. A point was classified as an outlier if its distance from the best-fit line was more than twice the weighted mean of the uncertainties in its 3T and 1.5T values.

RESULTS

Cardiac Results

Figure 1 shows typical cardiac images and the corresponding R2* maps at 1.5T and 3T from a patient with β-thalassemia major. Note that the signal in the heart decays more rapidly at 3T than at 1.5T, indicating a higher R2* value. Note also the radial variation in signal across the heart wall, with the subepicardium and subendocardium having lower intensity than the center of the myocardium. The R2* map confirms that the relaxation rate is higher in those regions. Similar patterns of increased R2* in the subepicardium or subendocardium were observed in seven of the patients but none of the control subjects. These observations are consistent with MRI findings by other investigators (16), and with autopsy analyses of iron distribution in patients with cardiac iron overload (17). For the purpose of comparison between 3T and 1.5T, R2* was evaluated from ROIs placed at the center of the septal myocardium, avoiding both right and left ventricular endocardial borders. The resulting R2* values for the patient shown in Fig. 1 were estimated as 80 ± 13 $second^{-1}$ at 1.5T and 163 ± 19 $second^{-1}$ at 3T.

Figure 2 shows 3T values of R2* in the myocardium plotted against the corresponding 1.5T values for both control subjects (blue diamonds) and patients (red squares). Figure 2a shows the complete data set, and Fig. 2b shows an enlargement of the inset. In each case the vertical axis spans twice the range of the horizontal axis. A total of 15 of the 20 control subjects exhibited cardiac R2* values that were tightly clustered at both field strengths. Over those 15 people the mean and SD were 23.4 ± 2.2 second^{-1} at 1.5T and 30.0 ± 3.7 second^{-1} at 3T. In four of the remaining control subjects the 3T values were significantly (>2 SD) higher than average (52 ± 10 second^{-1}, 53 ± 7 second^{-1}, 59 ± 7 second^{-1}, and 78 ± 6 second^{-1}), while the 1.5T values were within the normal range. In one subject the reverse was true, i.e., the 1.5T result was significantly higher than average (37 ± 5 second^{-1}), while the 3T result was within the normal range. All the image sets with anomalously high R2* values showed evidence of susceptibility artifacts, and all were acquired without the small volume shim. Figure 3 shows examples of cardiac images from one of these subjects. Note that the 3T image exhibits susceptibility artifacts while the corresponding 1.5T image appears to be artifact-free. The R2* value measured at 3T in this subject was 59 ± 7 second^{-1} (>2 SD above average), while the value at 1.5T was 20.6 ± 1.4 second^{-1} (within the normal range). Artifacts similar to those in Fig. 3 have been described previously, and are believed to be due to tissue-air susceptibility differences at the heart-lung interface (18).

Of the patients, five had cardiac R2* values within the normal range, as estimated from our control group (see Fig. 2b). The remaining nine patients had significantly higher R2* values, ranging from 63 ± 10 second^{-1} to 346 ± 37 second^{-1} at 1.5T, and from 108 ± 24 second^{-1} to 600 ± 100 second^{-1} at 3T. All these patients satisfied the currently accepted criterion for cardiac iron overload, namely a T2* value of less than 20 msec (i.e., R2* < 50 second^{-1}) at 1.5T (19). In the patient with the highest apparent cardiac iron overload, a single echo technique had to be applied at 3T to sample the short TE portion of the decay curve at submillisecond intervals.

The line of best fit to the cardiac data over all subjects (patients and controls) had a slope of 1.88 ± 0.14 and an intercept of −15 ± 4 second^{-1}. The five control subjects that exhibited anomalously high R2* values at one field strength were classified as outliers and excluded from the fitting procedure. These points have been circled in green on Fig. 2 for identification.

Liver Results

Figure 4 shows liver images and R2* maps from the same patient as in Fig. 1. Like the heart, the liver exhibits faster signal decay (higher R2*) at 3T than at 1.5T. The liver R2* values for this patient were 252 ± 9 second^{-1} at 1.5T and 480 ± 21 second^{-1} at 3T.

Figure 5 shows the 3T values of R2* in the liver plotted against the corresponding 1.5T values for control subjects and patients. Figure 5a shows the complete data set, and Fig. 5b shows an enlargement of the inset. Note that the scales are different from those used for the cardiac data, but the vertical axes still span twice the range of the horizontal axes. Over the control group, the mean and standard deviation of R2* in the liver were 39.2 ± 9.0 second^{-1} at 1.5T and 69.1 ± 21.9 second^{-1} at 3T. Three of the control subjects exhibited R2* values that were notably higher than the means (see Fig. 5b), but in each case the 1.5T and 3T values were correlated, suggesting that the cause was physiological rather than artifactual.

The liver R2* values among the patients ranged from 57 ± 2 second^{-1} to 1560 ± 120 second^{-1} at 1.5T. The lowest of these fell within the range measured in the control group, while the highest corresponds to an iron concentration of about 41 mg Fe/g tissue dry weight according to the calibration established by Wood et al (11). Four patients had sufficiently high iron concentration that it was necessary to use the single-echo technique to sample the short TE portion of the decay curve at submillisecond intervals. In one of these patients it was not

possible to obtain an R2* value at 3T because the signal intensity of the liver was less than twice the noise level at the minimum echo time (0.84 msec). This patient is therefore not represented in Fig. 5.

Over all subjects (patients and controls) the line of best fit to the 3T vs. 1.5T liver data had a slope of 2.00 ± 0.06 and an intercept of −11 ± 4 second^{-1}. Two points (circled in green) were classified as outliers and excluded from the fitting procedure. Both resulted from scans performed without the local shim, and may thus have been influenced by bulk susceptibility effects. Note that the remaining data points lie close to the line of best fit, even up to the highest iron concentrations for which both 1.5T and 3T values of R2* could be measured. The highest point on the graph had a 1.5T value of 1400 ± 90 second^{-1}, corresponding to an iron concentration of about 37 mg Fe/g tissue dry weight (11).

DISCUSSION

The cardiac R2* values in the control group were tightly clustered, with the exception of a few outlying points. Each of the outliers exhibited an anomalously high R2* value at only one field strength, while the value at the other field strength was within the normal range. This suggests that the outlying values were due to susceptibility artifacts. Inspection of the image sets in each case showed evidence of such artifacts, in the form of inhomogeneous or focal darkening across the myocardium. The fact that four of the five outlying values occurred at 3T may reflect a greater difficulty in shimming at the higher field strength. Our results suggest that performing a local small-volume shim may help to resolve this problem. Acquisition of a three-dimensional (3D) field map may also assist in the identification and possibly the correction of bulk susceptibility effects (20).

Over the control group the mean hepatic R2* value at 1.5T agreed with previously reported findings (11). The spread in R2* values among the control subjects was larger in the liver than the heart, with three people (all male) having liver R2* values that were significantly higher than the mean at both field strengths. Two of those subjects (aged 38 and 41) were substantially older than the other men in the cohort, so their higher R2* may be attributable in part to age-related iron accumulation. Other possible explanations include genetic factors or a prior history of blood transfusions. The Centers for Disease Control estimate that between 1% and 6% of people in the United States have some iron overloading as measured by elevated transferrin saturation levels. The majority of cases are believed to be hereditary hemochromatosis due to mutations in the *HFE* gene, which codes for a transmembrane glycoprotein that modulates iron uptake. Only a small proportion of individuals who inherit the mutations, however, develop clinical symptoms of iron overload.

The combined R2* data from patients and control subjects exhibited a linear relationship between 3T and 1.5T in both the heart and the liver. In each case the line of best fit to the 3T vs. 1.5T data had a slope of two (to within measurement error) and a small negative intercept. These findings can be interpreted in terms of a simple model of the mechanisms underlying R2* relaxation as follows.

The value of R2* depends on intravoxel magnetic field inhomogeneities and microscopic dipole–dipole interactions between protons (21). In iron-overloaded tissue the former is the dominant contribution due to susceptibility differences between the hemosiderin deposits and surrounding parenchyma. Since hemosiderin is paramagnetic, the resulting inhomogeneities scale with the strength of the external field B_0. In the static dephasing regime (21), their contribution to the transverse relaxation is therefore also proportional to B_0,

$$R_{\text{inhom}}(B_0, C_{\text{Fe}}) = f(C_{\text{Fe}})\, B_0. \quad (1)$$

Here the function $f(C_{\text{Fe}})$ is used to denote the dependence of R_{inhom} on tissue iron concentration. In vivo studies suggest that it is linear over a wide range of iron concentrations (11).

Dipole–dipole interactions occur among neighboring spins, particularly between the two protons in each water molecule. Their contribution to the net relaxation rate is determined mainly by the rotational correlation time of the water molecules within the tissue matrix, and is largely independent of field strength (22,23). We will therefore denote it as a constant, $R_{\text{d-d}}$. It is expected to be approximately equal to the noniron component of R2.

Expressing the net relaxation rate R2* as the sum of R_{inhom} and $R_{\text{d-d}}$, we can write

$$R_2^*(B_0, C_{\text{Fe}}) = f(C_{\text{Fe}})\, B_0 + R_{\text{d-d}}. \quad (2)$$

According to this model, the relationship between the 3T and 1.5T values of R2* is simply

$$R_2^*(3\text{T}, C_{\text{Fe}}) = 2R_2^*(1.5\text{T}, C_{\text{Fe}}) - R_{\text{d-d}}. \quad (3)$$

Thus the model predicts that the line of best fit to the 3T-vs.-1.5T data should have a slope of 2 and a small negative intercept. This is consistent with our observations. The value of $R_{\text{d-d}}$ could be determined only roughly from our data, and was estimated as 11 ± 4 second^{-1} in the liver and 15 ± 4 second^{-1} in the heart. These values agree with measurements by Bulte et al (23) of the noniron component of R2 in the liver, which ranged from 10.4 to 14.5 second^{-1}.

The increase in R2* with field strength has been predicted theoretically (21) and observed experimentally (24,25) in other contexts. The fact that both R2* and SNR increase with field strength makes high field imaging an attractive option for applications such as functional MRI of the brain and kidney (25,26), both of which rely on blood oxygenation level dependent (BOLD) changes in R2*.

While the increased R2* sensitivity at 3T is advantageous for those applications, it poses a handicap for quantification of iron overload in certain transfusion-dependent patients. In some patients, liver iron concentrations can be so high that T2* values fall into the submillisecond range even at 1.5T. Measurement of such short relaxation times places stringent requirements on the minimum echo time and echo spacing. The increase in R2* (shortening of T2*) with field strength makes accurate quantification even more challenging at higher fields. For patients with extremely high iron overload, therefore, 1.5T would be preferable to 3T for R2* imaging.

In our study we adopted a single-echo approach for R2* measurement in patients with very high iron levels. This allowed the TE increment to be made arbitrarily small. The disadvantage compared to the MGRE technique was that multiple acquisitions over separate breathholds were required to obtain the necessary series of images. Some patients in our study who could have been scanned using the MGRE technique at 1.5T needed a single-echo approach at 3T. Even the single-echo method will fail, however, when the R2* value becomes so high that that the signal at the minimum echo time falls to near the noise level. This occurred at 3T for one of the patients in our study. Also, it is conceivable that tissue with heterogeneous iron distribution may exhibit a multiexponential R2* decay, and that the fastest R2* components may have decayed away before TE_{min}. To obtain accurate estimates of iron concentration in such situations it would be necessary to reduce the minimum echo time as well as the echo

spacing. This requires a different approach, such as the ultrashort TE (UTE) technique developed by Graeme Bydder's group (27). By using truncated RF excitation pulses and center-out radial sampling, the UTE technique achieves echo times in the range of microseconds.

Our study focused on the relationship between R2* values at 1.5T and 3T, and we did not investigate R2 values. This was due to the practical difficulties of implementing spin echo sequences in the chest and abdomen, where navigator techniques or long breath-holds are required to avoid motion artifacts. In vitro studies using animal models of iron overload (9, 23) have shown that R2 also varies linearly with field strength. In vivo studies of iron stores in the brain at 0.5T and 1.5T (28) have suggested that the field-dependent increase in R2 may be a specific measure of tissue ferritin.

In conclusion, our results demonstrate that assessment of cardiac and hepatic iron burden by R2* imaging is feasible at 3T, but less straightforward than at 1.5T because of the greater difficulty of shimming and the more stringent requirements placed on the echo times. Inadequate shimming can produce erroneously high values of R2*. The apparent scaling of the iron-dependent component of R2* with field strength means that shorter TEs are needed to quantify R2* at stronger fields. Extremely high tissue iron concentrations (greater than about 37 mg Fe/g dry weight) may not be quantifiable at 3T without specialized pulse sequences designed to achieve ultrashort echo times. Nevertheless, 3T scanners are becoming increasingly widespread, and some sites now have only 3T systems, so it is important to be able to interpret 3T relaxation rates in terms of tissue iron concentration. The present study represents a preliminary step towards that goal, by comparing R2* values at 3T with those at 1.5T, for which the calibration against iron concentration has already been established (11). The primary limitation of the study was the fact that the patient cohort was relatively small, and included only two people with an apparent hepatic iron concentration of greater than 30 mg Fe/g tissue dry weight. Further investigation will be needed to confirm the relationship between R2* values at 3T and 1.5T over a broad range of tissue iron concentrations.

Acknowledgments

We thank Ken Hwang, PhD (Applied Science Laboratory, GE Healthcare) for development of the MGRE sequence. This work was supported by the National Greek Orthodox Ladies Philoptochos Society (to C.K.R.) and Novartis Pharmaceuticals, Inc. (to A.A.T.).

Contract grant sponsor: National Greek Orthodox Ladies Philoptochos Society; Contract grant sponsor: Novartis Pharmaceuticals, Inc.

REFERENCES

1. Olivieri NF, Brittenham GM. Iron-chelating therapy and the treatment of thalassemia. Blood 1997;89:739–761. [PubMed: 9028304]
2. Wood JC, Enriquez C, Ghugre N, et al. Physiology and pathophysiology of iron cardiomyopathy in thalassemia. Ann NY Acad Sci 2005;1054:386–395. [PubMed: 16339687]
3. Borgna-Pignatti C, Cappellini MD, de Stefano P, et al. Survival and complications in thalassemia. Ann NY Acad Sci 2005;1054:40–47. [PubMed: 16339650]
4. Cohen AR, Galanello R, Pennell DJ, et al. Thalassemia [Review]. Hematology Am Soc Hematol Educ Program 2004:14–34. [PubMed: 15561674]
5. Villeneuve JP, Bilodeau M, Lepage R, et al. Variability in hepatic iron concentration measurement from needle-biopsy specimens. J Hepatol 1996;25:172–177. [PubMed: 8878778]
6. Wood JC, Tyszka JM, Carson S, et al. Myocardial iron loading in transfusion-dependent thalassemia and sickle cell disease. Blood 2004;103:1934–1936. [PubMed: 14630822]
7. Anderson LJ, Holden S, Davis B, et al. Cardiovascular T2-star (T2*) magnetic resonance for the early diagnosis of myocardial iron overload. Eur Heart J 2001;22:2171–2179. [PubMed: 11913479]

8. Ghugre NR, Coates TD, Nelson MD, et al. Mechanisms of tissue-iron relaxivity: nuclear magnetic resonance studies of human liver biopsy specimens. Magn Reson Med 2005;54:1185–1193. [PubMed: 16215963]
9. Gossuin Y, Burtea C, Monseux A, et al. Ferritin-induced relaxation in tissues: an in vitro study. J Magn Reson Imaging 2004;20:690–696. [PubMed: 15390148]
10. Pierre TG, Clark PR, Chua-anusorn W, et al. Noninvasive measurement and imaging of liver iron concentrations using proton magnetic resonance. Blood 2005;105:855–861. [PubMed: 15256427]
11. Wood JC, Enriquez C, Ghugre N, et al. MRI R2 and R2* mapping accurately estimates hepatic iron concentration in transfusion-dependent thalassemia and sickle cell disease patients. Blood 2005;106:1460–1465. [PubMed: 15860670]
12. Voskaridou E, Douskou M, Terpos E, et al. Magnetic resonance imaging in the evaluation of iron overload in patients with beta thalassaemia and sickle cell disease. Br J Haematol 2004;126:736–742. [PubMed: 15327528]
13. Alexopoulou E, Stripeli F, Baras, et al. R2 relaxometry with MRI for the quantification of tissue iron overload in beta-thalassemic patients. J Magn Reson Imaging 2006;23:163–170. [PubMed: 16374880]
14. Clark PR, Chua-anusorn W, Pierre T. Proton transverse relaxation rate (R2) images of liver tissue; mapping local tissue iron concentrations with MRI. Magn Reson Med 2003;49:572–575. [PubMed: 12594762]
15. Gudbjartsson H, Patz S. The Rician distribution of noisy MRI data. Magn Reson Med 1995;34:910–914. [PubMed: 8598820]
16. Ghugre NR, Enriquez CM, Coates TD, et al. Improved R2* measurements in myocardial iron overload. J Magn Reson Imaging 2006;23:9–16. [PubMed: 16329085]
17. Olson LJ, Edwards WD, McCall JT, et al. Cardiac iron deposition in idiopathic hemochromatosis: histologic and analytic assessment of 14 hearts from autopsy. J Am Coll Cardiol 1987;10:1239–1243. [PubMed: 3680791]
18. Atalay MK, Poncelet BP, Kantor HL, Brady TJ, Weisskoff RM. Cardiac susceptibility artifacts arising from the heart-lung interface. Magn Reson Med 2001;45:341–345. [PubMed: 11180442]
19. Pennell DJ. T2* magnetic resonance and myocardial iron in thalassemia. Ann NY Acad Sci 2005;1054:373–378. [PubMed: 16339685]
20. Hu W, Lin W. Cerebral oxygen extraction fraction and cerebral venous blood volume measurements using MRI: effects of magnetic field variation. Magn Reson Med 2002;47:958–966. [PubMed: 11979575]
21. Yablonskiy DA, Haacke EM. Theory of NMR signal behavior in magnetically inhomogeneous tissues: the static dephasing regime. Magn Reson Med 1994;32:749–763. [PubMed: 7869897]
22. Gore, JC.; Kennan, RP. Physical and physiological basis of magnetic relaxation. In: Stark, DD.; Bradley, WG., editors. Magnetic resonance imaging. 3rd edition. Mosby; St. Louis: 1999. p. 33-42.
23. Bulte JW, Miller GF, Vymazal J, et al. Hepatic hemosiderosis in non-human primates: quantification of liver iron using different field strengths. Magn Reson Med 1997;37:530–536. [PubMed: 9094074]
24. Gati JS, Menon RS, Ugurbil K, Rutt BK. Experimental determination of the BOLD field strength dependence in vessels and tissue. Magn Reson Med 1997;38:296–302. [PubMed: 9256111]
25. Tumkur S, Vu A, Li L, Prasad PV. Evaluation of intrarenal oxygenation at 3.0 T using 3-dimensional multiple gradient-recalled echo sequence. Invest Radiol 2006;41:181–184. [PubMed: 16428990]
26. Voss HU, Zevin JD, McCandliss BD. Functional MR imaging at 3.0 T versus 1.5 T: a practical review. Neuroimaging Clin N Am 2006;16:285–297. [PubMed: 16731367]
27. Hall-Craggs MA, Porter J, Gatehouse PD, Bydder GM. Ultrashort echo time (UTE) MRI of the spine in thalassaemia. Br J Radiol 2004;77:104–110. [PubMed: 15010381]
28. Bartzokis G, Aravagiri M, Oldendorf WH, Mintz J, Marder SR. Field dependent transverse relaxation rate increase may be a specific measure of tissue iron stores. Magn Reson Med 1993;29:459–464. [PubMed: 8464361]

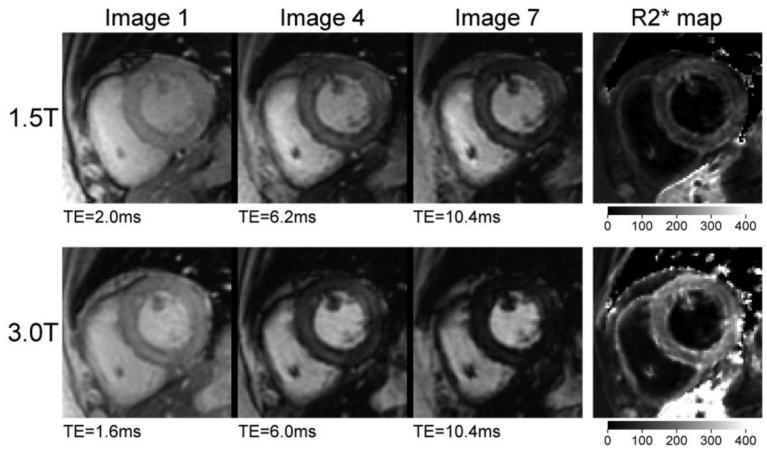

Figure 1.

Cardiac images and corresponding R2* maps at 1.5T and 3T from a patient with β-thalassemia. The first, fourth, and seventh images from the MGRE series are shown for each field strength. The window levels are kept constant across the three images in each series. The intensity scale bars are shown for the R2* maps in units of second^{-1}, and are identical for both field strengths.

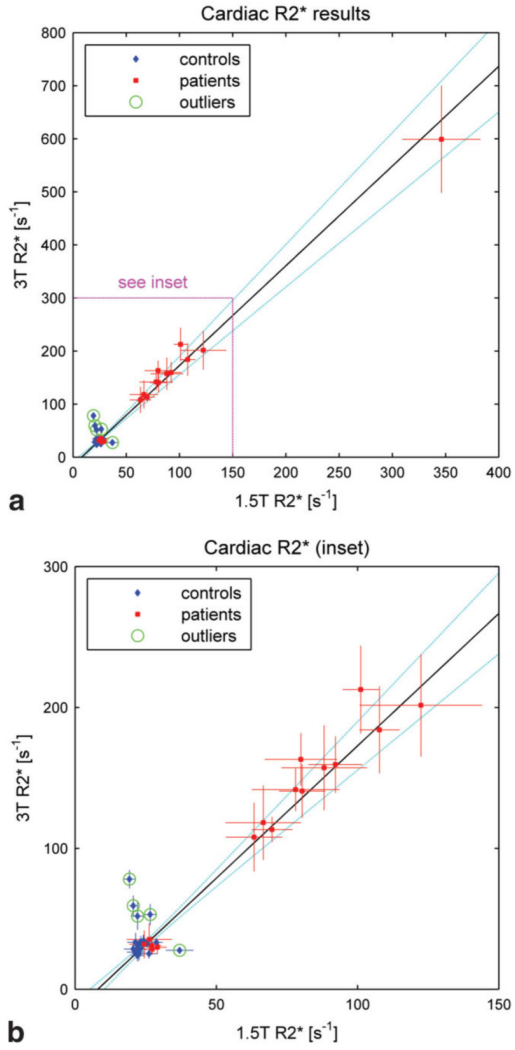

Figure 2.

3T vs. 1.5T values of R2* in the heart for control subjects (blue diamonds) and patients (red squares). **a:** The full data set. **b:** The inset in greater detail. Note that in each case the vertical axis (3T) spans twice the range of the horizontal axis (1.5T). The error bars for each subject indicate the standard deviation of R2* over the ROIs. The line of best fit is drawn in black and the 95% confidence interval (CI) is indicated by the dotted light blue curves. The green circles identify points that were classified as outliers and excluded from the analysis.

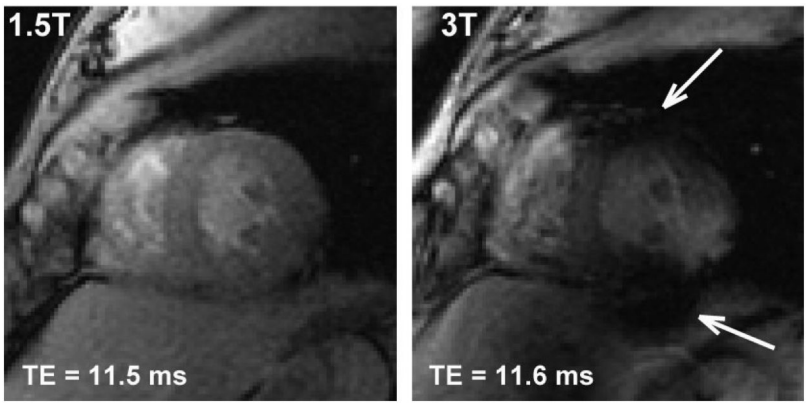

Figure 3.
1.5T and 3T images from a control subject whose cardiac data point was classified as an outlier. The 3T image exhibits susceptibility artifacts (arrows) near the heart-lung interface, while the 1.5T image appears to be artifact-free.

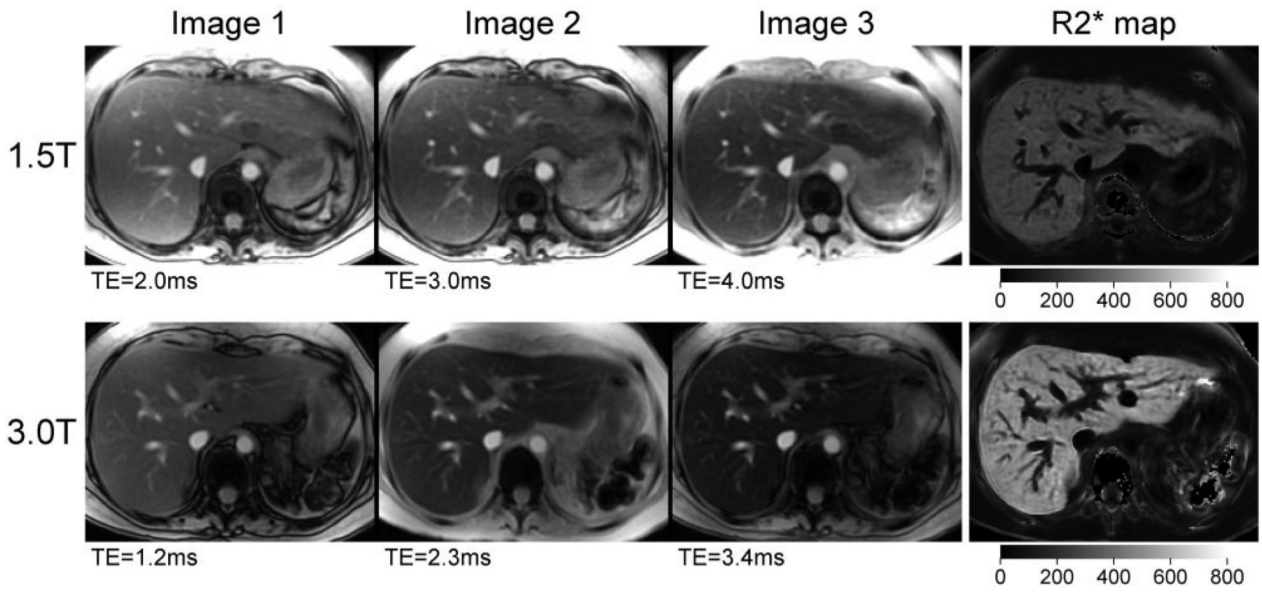

Figure 4.

Liver images and corresponding R2* maps at 1.5T and 3T from the same patient as in Fig. 1. The first three images from the MGRE series are shown for each field strength. The window levels are kept constant across the three images in each series. The intensity scale for the R2* maps is identical for both field strengths, but is different from that used in Fig. 1.

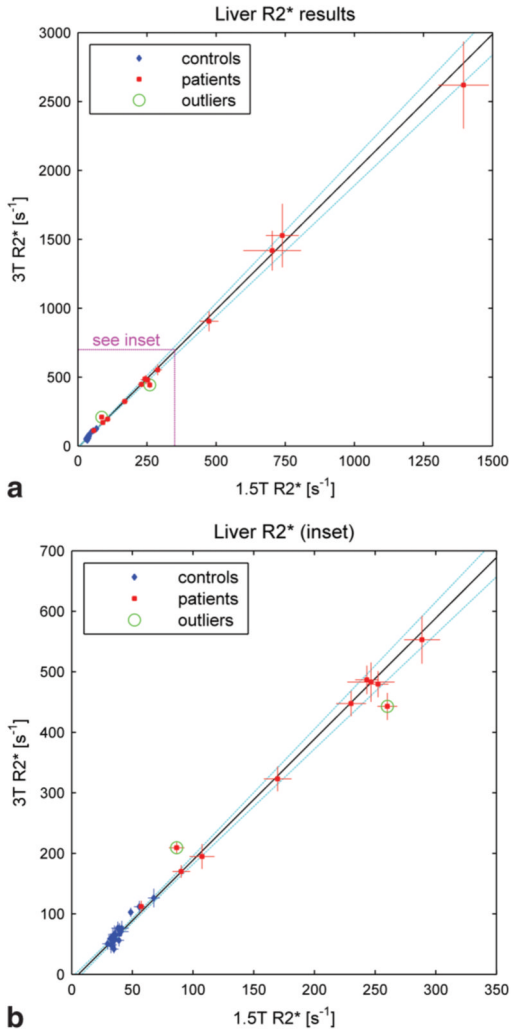

Figure 5.

3T vs. 1.5T values of R2* in the liver for control subjects (blue diamonds) and patients (red squares). **a:** The full data set. **b:** The inset in greater detail. Note that the scales are different from those used in Fig. 2, but the vertical axes (3T) still span twice the range of the horizontal axes (1.5T). The line of best fit is drawn in black and the 95% confidence interval (CI) is indicated by the dotted light blue curves. The green circles identify points that were classified as outliers and excluded from the best-fit analysis.